

Experimental simulation of Majorana-based quantum computation

Jin-Shi Xu,^{1,2,*} Kai Sun,^{1,2,*} Jiannis K. Pachos,³ Yong-Jian Han,^{1,2,†} Chuan-Feng Li,^{1,2,‡} and Guang-Can Guo^{1,2}

¹*CAS Key Laboratory of Quantum Information,
University of Science and Technology of China,
Hefei 230026, Peoples Republic of China*

²*Synergetic Innovation Center of Quantum Information and Quantum Physics,
University of Science and Technology of China,
Hefei 230026, Peoples Republic of China*

³*School of Physics and Astronomy,
University of Leeds, Leeds LS2 9JT, United Kingdom*

(Dated: December 3, 2024)

Abstract

Topological quantum computation aims to employ anyonic quasiparticles with exotic braiding statistics to encode and manipulate quantum information in a fault-tolerant way. Majorana zero modes are experimentally the simplest realisation of anyons that can non-trivially process quantum information. However, their braiding evolutions, necessary for realising topological gates, still remain beyond current technologies. Here we report the experimental encoding of four Majorana zero modes in an all-optical quantum simulator that give rise to a fault-tolerant qubit. We experimentally simulate their braiding and demonstrate both the non-Abelian character and the topological nature of the resulting geometric phase. We realise a full set of topological and non-topological gates that can arbitrarily rotate the encoded qubit. As an application, we implement the Deutsch-Jozsa algorithm exclusively by topological gates. Our experiment indicates the intriguing possibility of the experimental simulation of Majorana-based quantum computation with scalable technologies.

* These authors contributed equally to this work.

† smhan@ustc.edu.cn

‡ cfli@ustc.edu.cn

Quantum computers promise to perform particular tasks exponentially more efficient than their classical counterparts [1]. The key obstacle towards the realisation of a scalable quantum computer is overcoming environmental and control errors. A promising platform to build a fault-tolerant quantum computer is to use anyonic quasiparticles with non-Abelian statistics [2–4]. The non-local states of anyons can encode qubits that are unaffected by local environmental perturbations [5]. In addition, the logical quantum gates correspond to braiding evolutions of anyons that are inherently immune to control errors [3, 6].

In the past decades, non-Abelian anyons have been extensively theorised in condensed matter systems [7–10]. The most promising direction for realising non-Abelian anyons is the investigation on Majorana zero modes (MZMs). There are already several positive signatures for the realisation of MZMs in the laboratory [11–18]. Nevertheless, the experimental realisation of braiding operations is still a challenging open problem. Here, we report the quantum simulation of four MZMs in a network of two Kitaev chains and their braiding and dynamical evolutions. For that we encode the Kitaev Chain Model (KCM) that supports MZMs at its endpoints in an all-optical simulator [19]. The model encoding in our experiment is implemented in two steps. Firstly, we transform the fermion system to a spin-1/2 system through a Jordan-Wigner (JW) transformation [20, 21]. Secondly, we encode the spin-1/2 system into the spatial modes of single photons.

The optical simulation allows us to fully control the MZMs with a high fidelity. It is known that by braiding different pairs of MZMs we can realise only Clifford gates [22], such as the Hadamard gate, $H = \frac{1}{\sqrt{2}} \begin{pmatrix} 1 & -1 \\ 1 & 1 \end{pmatrix}$, the $(-\frac{\pi}{4})$ -phase gate, $R = \begin{pmatrix} 1 & 0 \\ 0 & -i \end{pmatrix}$, which are not universal for quantum computation [23]. The inclusion of a non-Clifford gate, such as the $\frac{\pi}{8}$ -phase gate, $T = \begin{pmatrix} 1 & 0 \\ 0 & e^{i\pi/4} \end{pmatrix}$, can resolve this problem [24]. We simulate the $\frac{\pi}{8}$ -phase gate by moving two MZMs at the same site and exposing them to a controlled local perturbation. We experimentally demonstrate that, unlike the H and the R topological gates, the $\frac{\pi}{8}$ -phase gate is not immune to local perturbations. Nevertheless, ‘magic state distillation’ [25] can be used to produce error-corrected $\frac{\pi}{8}$ -phase gates from noisy ones. This approach permits an impressive high error threshold, over 0.141 [22], for noisy gates. In addition, recent results show that the number of non-topological $\frac{\pi}{8}$ -phase gates can be dramatically reduced in quantum algorithms [26, 27], which significantly improves the overall fault-tolerance of

MZM quantum computation. We finally implement the Deutsch-Jozsa algorithm [28], which requires only the application of H and R gates on a single qubit encoded in MZMs and is thus topologically protected at all times [29]. When access to an arbitrary number of Kitaev chains is possible, two-qubit topological gates can be realised by employing the braiding control procedures presented here.

UNIVERSAL QUANTUM COMPUTATION WITH MAJORANA ZERO MODES

The smallest system of two connected Kitaev chains that remains fault-tolerant against local perturbations at all times during the braiding evolution comprises of six fermion sites [30]. Using six rather than five sites guarantees that no pairs of MZMs ever meet at the same site (see Supplementary Information Figs. S1 and S2). Here we describe these fermions through the canonical operators c_j and c_j^\dagger , with positions $j = 1, \dots, 6$, where $j = 1, 2$ constitutes the first chain, $j = 4, 5, 6$ constitutes the second and $j = 3$ corresponds to the link between them, as shown in Fig. 1. The Kitaev model for the two chains is given in terms of Majorana operators, $\gamma_{ja} = c_j + c_j^\dagger$ and $\gamma_{jb} = i(c_j^\dagger - c_j)$, by the Hamiltonian

$$H_{M_0} = i(\gamma_{1b}\gamma_{2a} + \gamma_{4b}\gamma_{5a} + \gamma_{5b}\gamma_{6a}) + i\gamma_{3a}\gamma_{3b}. \quad (1)$$

The Majorana operators γ_m satisfy the relations $\gamma_m^\dagger = \gamma_m$ and $\gamma_l\gamma_m + \gamma_m\gamma_l = 2\delta_{lm}$ for $l, m = 1a, 1b, \dots, 6a, 6b$. Note that the particular operators $\gamma_{1a}, \gamma_{2b}, \gamma_{4a}$ and γ_{6b} are not present in Hamiltonian (1), so $[H_{M_0}, \gamma_j] = 0$ for $j = 1a, 2b, 4a, 6b$. As a result, these Majorana modes have zero energy, giving rise to four endpoint MZMs, denoted as A, B, C and D in Fig. 1. The logical qubit states are taken to be $|0_L\rangle = |00_g\rangle$ and $|1_L\rangle = |11_g\rangle$ corresponding to the degenerate ground-states of H_{M_0} with even fermion parity, given by $|00_g\rangle = N f_1 d_1 f_2 d_2 d_3 |\text{vac}\rangle$ and $|11_g\rangle = N f_1^\dagger f_2^\dagger |00_g\rangle$, where $f_1 = (\gamma_{1a} + i\gamma_{2b})/2$, $f_2 = (\gamma_{6b} + i\gamma_{4a})/2$, $d_1 = (\gamma_{1b} + i\gamma_{2a})/2$, $d_2 = (\gamma_{4b} + i\gamma_{5a})/2$ and $d_3 = (\gamma_{5b} + i\gamma_{6a})/2$. For convenience we denote the appropriate normalisation constant by N (see Methods).

The Hadamard gate H on the logical qubit can be realised by anticlockwise braiding the MZMs A and C positioned at sites 1 and 4, respectively. The transport of the MZMs around the chain network is performed by adiabatically evolving the system through the following

sequence of Hamiltonians, H_{M_0} , H_{h_1} , H_{h_2} , H_{h_3} and H_{M_0} , where

$$\begin{aligned} H_{h_1} &= i(\gamma_{1b}\gamma_{2a} + \gamma_{1a}\gamma_{3a} + \gamma_{5b}\gamma_{6a}) + i\gamma_{4a}\gamma_{4b}, \\ H_{h_2} &= i(\gamma_{1b}\gamma_{2a} + \gamma_{1a}\gamma_{3a} + \gamma_{3b}\gamma_{4b} + \gamma_{5b}\gamma_{6a}), \\ H_{h_3} &= i(\gamma_{1b}\gamma_{2a} + \gamma_{1a}\gamma_{3a} + \gamma_{4b}\gamma_{5a} + \gamma_{5b}\gamma_{6a}). \end{aligned} \quad (2)$$

A depiction of the resulting MZMs transportation is shown in the Supplementary Information (Fig. S1). The ground states of these Hamiltonians have the MZMs located at the desired sites. Hence, braiding can be implemented by a set of consecutive imaginary-time evolution (ITE) operators, $e^{-H_{M_0}t}$, $e^{-H_{h_1}t}$, $e^{-H_{h_2}t}$, $e^{-H_{h_3}t}$ and $e^{-H_{M_0}t}$, where t is taken to be large enough for these operators to faithfully represent projectors onto the corresponding ground states [31]. The resulting evolution can be written in the logical basis $\{|00_g\rangle, |11_g\rangle\}$

as $H = \frac{1}{\sqrt{2}} \begin{pmatrix} 1 & -1 \\ 1 & 1 \end{pmatrix}$ (see Methods for details).

To realise the R gate on the logical qubit we need to anticlockwise braid the MZMs C and D. The braiding is performed by switching between the corresponding Hamiltonians H_{r_1} , H_{r_2} and H_{r_3} (details can be found in the Supplementary Information). This time evolution can be implemented by a set of consecutive ITE operators, $e^{-H_{M_0}t}$, $e^{-H_{r_1}t}$, $e^{-H_{r_2}t}$, $e^{-H_{r_3}t}$ and $e^{-H_{M_0}t}$. The resulting effective evolution is given by $R = \begin{pmatrix} 1 & 0 \\ 0 & -i \end{pmatrix}$ in the logical basis.

The Hermitian conjugate gates, H^\dagger and R^\dagger , are produced by reversing the orientation of the exchanging paths. Realising the Hadamard gate, H, and the $(-\frac{\pi}{4})$ -phase gate, R, by braiding MZMs demonstrates the non-Abelian character of the MZMs. When these two operations are performed in reverse order, they give a different composite statistical evolution, since $HR \neq RH$.

To realise the $\frac{\pi}{8}$ -phase gate we place two MZMs at the same site and apply a local field. This causes the splitting of the ground state degeneracy for a certain time, during which the appropriate phase factor is accumulated [24]. In particular, we transport the B and C MZMs to site 3 by a set of ITE operations. Then the population dependent Hamiltonian $H_e = -i\gamma_{3a}\gamma_{3b}$ is operated for a certain time τ , as shown in Fig. 1c. Finally, the MZMs are transferred back to their initial position. The details of this process can be found in the Supplementary Information. During this evolution, the qubit states are transformed by

$M = \begin{pmatrix} \cos \tau & -i \sin \tau \\ -i \sin \tau & \cos \tau \end{pmatrix} = e^{-i\sigma_x \tau}$. With the help of the Hadamard gate we can obtain

the $\frac{\pi}{8}$ -phase gate as $H^\dagger M H = e^{-i\tau} \begin{pmatrix} 1 & 0 \\ 0 & e^{2i\tau} \end{pmatrix}$. Thus, the $\frac{\pi}{8}$ -phase gate can be achieved by choosing the time to be $\tau = \frac{\pi}{8}$. This gate is not protected against noise perturbations acting on site 3 when both MZMs are positioned there. Moreover, unlike the braiding gates, the dynamical gate is sensitive to timing errors.

During the realisation of the H and R topological gates the braided MZMs are never positioned at the same site. So these gates are immune to arbitrary single-site perturbative errors. The $\frac{\pi}{8}$ -phase gate is not expected to be resilient against perturbations that act on site 3, where the two MZMs are brought together. Such perturbations can lift the degeneracy of the logical basis states thereby causing dephasing of the encoded quantum information. Nevertheless, the contributions of sufficiently random perturbations cancel out algebraically. We experimentally simulate the influence of a variety of noise patterns during the implementation of the $\frac{\pi}{8}$ -phase gate and report their effect on the fidelity of the topologically encoded information.

Intriguingly, the Deutsch-Jozsa algorithm [28] can be performed exclusively by non-universal braiding evolutions [29] and thus it can be realised in a topologically fault-tolerant way. The process for implementing the Deutsch-Jozsa algorithm on a single qubit is shown in Fig. 1d. The required Hadamard gate operation can be realised by exchanging the MZMs A and C, while the unitary operation U_f is either the identity gate (do nothing) or the σ_z gate, realised by two successive braidings of C and D. A detailed description of the Deutsch-Jozsa algorithm can be found in the Supplementary Information.

EXPERIMENTAL SETUP

To simulate the braiding evolutions of MZMs we transform the fermionic Hamiltonians H_{M_0} , H_{h_1} , H_{h_2} and H_{h_3} , via a JW transformation, into the equivalent spin Hamiltonians, H_0 , H_1 , H_2 and H_3 , respectively, where

$$\begin{aligned}
 H_0 &= -\sigma_1^x \sigma_2^x + \sigma_3^z - \sigma_4^x \sigma_5^x - \sigma_5^x \sigma_6^x, \\
 H_1 &= -\sigma_1^x \sigma_2^x + \sigma_1^y \sigma_2^z \sigma_3^x + \sigma_4^z - \sigma_5^x \sigma_6^x, \\
 H_2 &= -\sigma_1^x \sigma_2^x + \sigma_1^y \sigma_2^z \sigma_3^x + \sigma_3^x \sigma_4^y - \sigma_5^x \sigma_6^x, \\
 H_3 &= -\sigma_1^x \sigma_2^x + \sigma_1^y \sigma_2^z \sigma_3^x - \sigma_4^x \sigma_5^x - \sigma_5^x \sigma_6^x.
 \end{aligned} \tag{3}$$

During the adiabatic process the spin system has the same spectrum as the fermion system at all times. Hence, both systems share the same evolution operators when written in their corresponding basis [21, 31] (see Methods). In particular, the transport of MZMs can be faithfully studied in the equivalent spin system. Due to the commutation relations between the terms of H_0 , H_1 , H_2 and H_3 , the total process of ITE can be further simplified to be $e^{-H_0 t} e^{-H_3 t} e^{-H_2 t} e^{-H_1 t} |\phi_0\rangle = e^{-\sigma_3^z t} e^{\sigma_4^x \sigma_3^x t} e^{-\sigma_3^x \sigma_4^y t} e^{-\sigma_1^y \sigma_2^z \sigma_3^x t} e^{-\sigma_4^z t} |\phi_0\rangle$, where $|\phi_0\rangle$ is the ground state of H_0 (see Methods). To simulate the above dynamics, we need, in principle, a 2^7 -dimensional Hilbert space, that corresponds to six spins for the chain network and an extra spin for implementing dissipation. However, due to the character of the ITE, we need to focus only on manipulations that act on the low-energy subspace, which is 2^5 -dimensional.

The experimental setup that realises the braiding evolution of MZMs A and C is shown in Fig. 2a. We encode the quantum states in the optical spatial modes of photons and manipulate them by beam displacers (BDs). A beam displacer is a birefringent crystal, which separates light beams with horizontal and vertical polarisations by a certain displacement that depends on the length of the crystal [32]. Different settings of the optical axis of BDs, result in the light beams being separated in different directions. In our experiment, the polarisation of the photons is used as the environmental degree of freedom for the realisation of the ITE operations. The coupling between the spatial modes and the photon polarisation is achieved using half-wave plates (HWPs), which rotate the polarisation of the corresponding modes. Quarter-wave plates (QWPs) are used to introduce the desired relative phases. Combinations of HWPs and QWPs can be used to rotate the basis of the states to the corresponding Hamiltonian. A dissipative evolution is accomplished in two steps. Initially, photons are passed through a polarising beam splitter (PBS), which transmits the horizontal component and reflects the vertical one. Subsequently, photons with vertical polarisation are completely dissipated and only the ones with horizontal polarisation are preserved. The resulting states correspond to the ground state of the spin chain system. In this way, the state $|\phi_0\rangle$ is initially prepared and is then sent to the ITE operation of H_1 , H_2 , H_3 and H_0 for the braiding of A and C. Each of the ITE operations, are shown in the amplified panels in Fig. 2a, including an illustration of the basis rotations and the dissipative evolutions. During the experiment, we need to construct a stable interferometer with eight spatial modes. The effective operator of our setup is reconstructed by quantum process tomography with 256 measurements [33].

The experimental configurations that demonstrate the braiding of C and D and the $\frac{\pi}{8}$ -phase gate are similar to the one shown in Fig. 2a and are given in the Supplementary Information. We further investigate the robustness against noise of the $\frac{\pi}{8}$ -phase gate. Two different types of errors are considered, the phase error realised by the spin operation $(1 + \sigma^z)/2$ and the flip error realised by $(\sigma^y\sigma^y + \sigma^x\sigma^x)/2$ (details in Supplementary Information). The experimental configurations that realise these errors are shown in Figs. 2b and c.

Realisation of gate operations and implementation of the Deutsch-Jozsa algorithm

In order to identify the quantum gates resulting from the braiding of MZMs, we express the data in the logical basis $\{|00_g\rangle, |11_g\rangle\}$. The transformation between the logical basis and the eigenstates of H_0 is shown in the Methods. The operators can be described in the 4-dimensional basis $\{I, X, Y, Z\}$, where I represents the identity and where X, Y and Z represent the three Pauli operators σ^x , σ^y and σ^z , respectively. The experimental result for the implementation of $H = (I - iY)/\sqrt{2}$ is shown in Figs. 3a (real part) and b (imaginary part). The overall fidelity of the braiding operator is $93.47 \pm 0.02\%$. For the $\frac{\pi}{8}$ -phase gate, $T = \cos \frac{\pi}{8}I - i \sin \frac{\pi}{8}Z$, the experimental fidelity is $92.57 \pm 0.01\%$. The real and imaginary parts of the density matrix are shown in Fig. 4a and b. The $(-\frac{\pi}{4})$ -phase gate, $R = \cos \frac{\pi}{4}I + i \sin \frac{\pi}{4}Z$, is further demonstrated with a fidelity of $93.44 \pm 0.01\%$. The whole density matrices in the basis of $\{|00_g\rangle, |01_g\rangle, |10_g\rangle, |11_g\rangle\}$ corresponding to these operations are given in the Supplementary Information.

With these gates in hand, the Deutsch-Jozsa algorithm, shown in Fig. 1d, can be demonstrated in the following way. First we prepare the input state $|00_g\rangle$. If the operation in the box is the identity (constant function), the braiding operation of U_{AC} (braiding MZMs A and C) is implemented twice directly on the input state. The final state can be written as $U_{AC}U_{AC}|00_g\rangle = |11_g\rangle$, which corresponds to implementing the $H \cdot I \cdot H$ gate operations. If the operation in the box is σ^z (balanced function), the final state becomes $U_{AC}U_{CD}U_{CD}U_{AC}|00_g\rangle = |00_g\rangle$, where U_{CD} corresponds to the braiding of C and D. These gate operations can be written as $H \cdot R^2 \cdot H$. In our experiment, the output states, denoted as ρ_c^e and ρ_b^e for constant and balanced operations, respectively, are directly calculated from the experimentally reconstructed operators U_{AC} and U_{CD} . The state evolution during the operation of the Deutsch-Jozsa algorithm are shown in Figs. 3e and f, where the black dots

TABLE I. Experimentally determined final state fidelities for different gate operations.

Input	Hadamard	$(-\frac{\pi}{4})$-phase	$\frac{\pi}{8}$-phase
$ 00_g\rangle$	96.14(1)%	99.43(1)%	99.39(2)%
$ 11_g\rangle$	98.81(1)%	98.49(1)%	99.16(2)%
$(00_g\rangle - i 11_g\rangle)/\sqrt{2}$	98.69(2)%	99.28(1)%	98.16(3)%
$(00_g\rangle + 11_g\rangle)/\sqrt{2}$	99.07(1)%	99.78(1)%	99.29(1)%

and the coloured dots represent the corresponding theoretical and experimental results, respectively. The corresponding braiding patterns with isolated MZMs A, B, C, and D are shown in Figs. 3c and d.

Table I shows the experimentally determined final state fidelities for different gate operations. The input states are $|00_g\rangle$, $|11_g\rangle$, $(|00_g\rangle - i|11_g\rangle)/\sqrt{2}$ and $(|00_g\rangle + |11_g\rangle)/\sqrt{2}$. For the Hadamard gate, H, the final states correspond to $(|00_g\rangle + |11_g\rangle)/\sqrt{2}$, $(|00_g\rangle - |11_g\rangle)/\sqrt{2}$, $(|00_g\rangle - i|11_g\rangle)/\sqrt{2}$ and $|11_g\rangle$, respectively. For the $(-\frac{\pi}{4})$ -phase gate, R, the final states correspond to $|00_g\rangle$, $|11_g\rangle$, $(|00_g\rangle - |11_g\rangle)/\sqrt{2}$ and $(|00_g\rangle - i|11_g\rangle)/\sqrt{2}$. For the $\frac{\pi}{8}$ -phase gate, T, the final states correspond to $\cos\frac{\pi}{8}|00_g\rangle - i\sin\frac{\pi}{8}|11_g\rangle$, $\sin\frac{\pi}{8}|00_g\rangle + i\cos\frac{\pi}{8}|11_g\rangle$, $[(\cos\frac{\pi}{8} - \sin\frac{\pi}{8})|00_g\rangle - i(\cos\frac{\pi}{8} + \sin\frac{\pi}{8})|11_g\rangle]/\sqrt{2}$ and $[(\cos\frac{\pi}{8} - i\sin\frac{\pi}{8})|00_g\rangle + (\cos\frac{\pi}{8} - i\sin\frac{\pi}{8})|11_g\rangle]/\sqrt{2}$. The final state fidelities are all above 96%. This result shows the high quality of the optical setup. The errors of the fidelities are estimated from the counting statistics.

Fault-tolerance of quantum gates in the presence of noise

We now experimentally investigate the influence of noise during the implementation of the gate operations. More concretely, we add phase errors and flip errors on different sites during the control operations that give the $\frac{\pi}{8}$ -phase gate. The effective one-qubit gates in our scheme act on the space spanned by $\{|00_g\rangle, |11_g\rangle\}$. Fig. 4 shows the final experimental density matrices with errors on different sites. For comparison, Figs. 4a and b show the real and imaginary parts of the density matrix after the implementation of the $\frac{\pi}{8}$ -phase gate without adding any errors at all. When local phase errors happen on site 4 during the gate manipulations, only one MZM is disturbed at a time and the operation remains unaffected. This resilience of the encoded information is clearly shown in Figs. 4c and d. On the other hand, when the phase error is implemented on site 3, both MZMs are simultaneously

disturbed. Hence, the final state is corrupted as it is no longer topologically protected. A detailed analysis is given in the Supplementary Information.

Besides phase errors, we also consider flip errors. In the fermionic system a flip error happens when a fermion erroneously tunnels between neighbouring sites [30]. This evolution can be exponentially suppressed by increasing the potential barrier between the two sites. Flip errors degrade the encoded information, if the MZMs are positioned on the same or on neighbouring sites to where the flip error acts. If the flip error acts on sites that are not occupied by MZMs then the encoded information remains intact. To demonstrate this, we implement a flip error between sites 4 and 5 when the MZMs are both on site 3. In this case the operation remains unchanged, as shown in Figs. 4e and f. However, if the flip error acts on sites 3 and 4 while both MZMs are positioned on site 3, then the operation is corrupted, as shown in Figs. 4g and h.

CONCLUSIONS AND DISCUSSION

In summary, we have experimentally demonstrated that it is in principle possible to implement fault-tolerant quantum computation with MZMs. Our quantum simulation is based on the dissipation method for the implementation of the geometric phase introduced in our previous work [31]. There we experimentally simulate a single Kitaev chain and demonstrate the Abelian braiding statistics of its two endpoint MZMs. Here we employ two chains with four endpoint MZMs to encode a single topological qubit. We find that the experimentally obtained geometric phases are non-Abelian and topological in agreement with the braiding statistics of MZMs. We realised the basic Hadamard gate, H , and $(-\frac{\pi}{4})$ -phase gate, R , by simulating the braiding of MZMs. The $\frac{\pi}{8}$ -phase gate is demonstrated by moving two MZMs to the same site and subjecting them to population dependent realtime evolution by turning on a local chemical potential.

Due to the specific nature of our optical simulator we are able to perform control operations with very high fidelity, but the scalability of our system is limited. However, when more than two Kitaev chains are available, full-scale topological quantum computation with MZMs can be performed by employing exactly the same control procedures demonstrated here, applied to arbitrary pairs of chains. Scalable MZM quantum computation can be achieved by translating our photonic simulator implementation to scalable systems, such as

ion traps [34] or ultracold atoms [35] technologies, where the ITE dissipation methods have already been established.

METHODS

Performing imaginary-time evolution. Any pure state $|\phi\rangle$ can be expressed in a complete set of eigenstates $|e_k\rangle$ of a certain Hamiltonian H as $|\phi\rangle = \sum_k q_k |e_k\rangle$, where q_k 's represent the corresponding complex amplitudes. The ITE operator associated to H is given by $\exp(-Ht) \sum_k q_k |e_k\rangle = \sum_k q_k \exp(-E_k t) |e_k\rangle$, where E_k is the eigenvalue corresponding to $|e_k\rangle$. After the ITE, the amplitude q_k is changed to $q_k \exp(-E_k t)$. The decay of the amplitude depends exponentially on the energy: the higher the energy, the faster the decay of the amplitude. Therefore, only the ground states (with lowest energy) survive for large times t . The evolution time t is chosen to be long enough to drive the input state to the ground state of H with high fidelity.

The implementation of the ITE operations, employed to perform the braiding, can be simplified as the terms of the corresponding Hamiltonians commute with each other. For example, $e^{-H_0 t}$ can be decomposed into $e^{\sigma_5^z \sigma_6^x t} e^{-\sigma_3^z t} e^{\sigma_4^x \sigma_5^z t} e^{\sigma_1^x \sigma_2^z t}$. The ITE operator of each term can be directly implemented by local unitary operations and dissipation. To perform the dissipation in a controlled way, an environmental degree of freedom is introduced and it is appropriately coupled to the system. The total state of the system and its environment can be written as $|\phi_t\rangle = (|\phi_g\rangle|0_e\rangle + |\phi_g^\perp\rangle|1_e\rangle)/\sqrt{2}$, where $|\phi_g^\perp\rangle$ denotes the states that are orthogonal to the ground state $|\phi_g\rangle$ of the system. The environmental state $|1_e\rangle$ is dissipated during the evolution, and only $|0_e\rangle$ is preserved. Therefore, the ground state of the corresponding Hamiltonian is obtained.

Encoding logical qubits in physical states. For the two-chain Kitaev model with a total of six fermions, we define the two basis of the ground-state space of the first chain comprised by the fermion 1 and 2 as $|0_{12f}\rangle = -i\sqrt{2}f_1 d_1 |\text{vac}\rangle = (1 + c_1^\dagger c_2^\dagger) |\text{vac}\rangle/\sqrt{2}$ and $|1_{12f}\rangle = f_1^\dagger |0_{12g}\rangle = (c_2^\dagger + c_1^\dagger) |\text{vac}\rangle/\sqrt{2}$, where $f_1 = (\gamma_{1a} + i\gamma_{2b})/2$, $d_1 = (\gamma_{1b} + i\gamma_{2a})/2$. In the same way, we define the basis in the ground-state space of the chain comprised by the fermion 4, 5 and 6 as $|1_{456f}\rangle = 2f_2 d_2 d_3 |\text{vac}\rangle = -\frac{i}{2}(c_4^\dagger c_5^\dagger c_6^\dagger + c_4^\dagger + c_5^\dagger + c_6^\dagger) |\text{vac}\rangle$ and $|0_{456f}\rangle = f_2^\dagger |1_{456g}\rangle = -\frac{i}{2}(I + c_4^\dagger c_5^\dagger + c_4^\dagger c_6^\dagger + c_5^\dagger c_6^\dagger) |\text{vac}\rangle$, where $f_2 = (\gamma_{6b} + i\gamma_{4a})/2$, $d_2 = (\gamma_{4b} + i\gamma_{5a})/2$ and $d_3 = (\gamma_{5b} + i\gamma_{6a})/2$.

Under the JW transformation the MZMs can be faithfully studied in the equivalent spin system. The ground states of Hamiltonians (3) can be expressed in terms of the eigenvectors $\{|x\rangle, |\bar{x}\rangle\}$, $\{|y\rangle, |\bar{y}\rangle\}$ and $\{|z\rangle, |\bar{z}\rangle\}$ of the Pauli operators σ^x , σ^y and σ^z , respectively. By

defining the vacuum states as $|\text{vac}_{12}\rangle = |\bar{z}_1\bar{z}_2\rangle$ and $|\text{vac}_{456}\rangle = |\bar{z}_4\bar{z}_5\bar{z}_6\rangle$, the corresponding states of the spin system are given by $|0_{12f}\rangle \leftrightarrow |0_{12}\rangle = (|\bar{z}_1\bar{z}_2\rangle + |z_1z_2\rangle)/\sqrt{2}$, $|1_{12f}\rangle \leftrightarrow |1_{12}\rangle = (|z_1\bar{z}_2\rangle + |\bar{z}_1z_2\rangle)/\sqrt{2}$, $|1_{456f}\rangle \leftrightarrow |1_{456}\rangle = (|z_4z_5z_6\rangle + |z_4\bar{z}_5\bar{z}_6\rangle + |\bar{z}_4z_5\bar{z}_6\rangle + |\bar{z}_4\bar{z}_5z_6\rangle)/2$ and $|0_{456f}\rangle \leftrightarrow |0_{456}\rangle = (|\bar{z}_4\bar{z}_5\bar{z}_6\rangle + |z_4z_5\bar{z}_6\rangle + |z_4\bar{z}_5z_6\rangle + |\bar{z}_4z_5z_6\rangle)/2$.

Under these transformations we have, $|x_1x_2\rangle = (|0_{12}\rangle + |1_{12}\rangle)/\sqrt{2}$, $|\bar{x}_1\bar{x}_2\rangle = (|0_{12}\rangle - |1_{12}\rangle)/\sqrt{2}$, $|x_4x_5x_6\rangle = (|0_{456}\rangle + |1_{456}\rangle)/\sqrt{2}$ and $|\bar{x}_4\bar{x}_5\bar{x}_6\rangle = (|1_{456}\rangle - |0_{456}\rangle)/\sqrt{2}$. Using the same notation for the corresponding logical basis in the fermionic and the spin systems we define the logical basis as $|00_g\rangle = |0_{12}0_{456}\rangle|\bar{z}_3\rangle$, $|01_g\rangle = |0_{12}1_{456}\rangle|\bar{z}_3\rangle$, $|10_g\rangle = |1_{12}0_{456}\rangle|\bar{z}_3\rangle$ and $|11_g\rangle = |1_{12}1_{456}\rangle|\bar{z}_3\rangle$. The transformation between the X, Y and Z basis and the logic basis is given by

$$\begin{pmatrix} |x_1x_2\bar{z}_3x_4x_5x_6\rangle \\ |x_1x_2\bar{z}_3\bar{x}_4\bar{x}_5\bar{x}_6\rangle \\ |\bar{x}_1\bar{x}_2\bar{z}_3x_4x_5x_6\rangle \\ |\bar{x}_1\bar{x}_2\bar{z}_3\bar{x}_4\bar{x}_5\bar{x}_6\rangle \end{pmatrix} = \frac{1}{2} \begin{pmatrix} 1 & 1 & 1 & 1 \\ -1 & 1 & -1 & 1 \\ 1 & 1 & -1 & -1 \\ -1 & 1 & 1 & -1 \end{pmatrix} \begin{pmatrix} |00_g\rangle \\ |01_g\rangle \\ |10_g\rangle \\ |11_g\rangle \end{pmatrix}. \quad (4)$$

By omitting for simplicity normalisation factors, the ground state of H_0 can be expressed as

$$\begin{aligned} |\phi_0\rangle &= \alpha|x_1x_2\bar{z}_3x_4x_5x_6\rangle + \beta|\bar{x}_1\bar{x}_2\bar{z}_3x_4x_5x_6\rangle + \mu|x_1x_2\bar{z}_3\bar{x}_4\bar{x}_5\bar{x}_6\rangle + \nu|\bar{x}_1\bar{x}_2\bar{z}_3\bar{x}_4\bar{x}_5\bar{x}_6\rangle \\ &= (\alpha + \beta - \mu - \nu)|00_g\rangle + (\alpha + \beta + \mu + \nu)|01_g\rangle \\ &\quad + (\alpha - \beta - \mu + \nu)|10_g\rangle + (\alpha - \beta + \mu - \nu)|11_g\rangle. \end{aligned} \quad (5)$$

After the braiding evolution between the A and C MZMs, the final state becomes

$$\begin{aligned} |\phi_4\rangle &= (\alpha + \beta)|x_1x_2\bar{z}_3x_4x_5x_6\rangle + (\mu - \nu)|x_1x_2\bar{z}_3\bar{x}_4\bar{x}_5\bar{x}_6\rangle \\ &\quad + (\beta - \alpha)|\bar{x}_1\bar{x}_2\bar{z}_3x_4x_5x_6\rangle + (\mu + \nu)|\bar{x}_1\bar{x}_2\bar{z}_3\bar{x}_4\bar{x}_5\bar{x}_6\rangle \\ &= (\beta - \mu)|00_g\rangle + (\beta + \mu)|01_g\rangle + (\alpha + \nu)|10_g\rangle + (\alpha - \nu)|11_g\rangle. \end{aligned} \quad (6)$$

As a result, the unitary transformation associated to the braiding evolution becomes

$$U = \frac{1}{\sqrt{2}} \begin{pmatrix} 1 & 0 & 0 & -1 \\ 0 & 1 & -1 & 0 \\ 0 & 1 & 1 & 0 \\ 1 & 0 & 0 & 1 \end{pmatrix}. \quad (7)$$

If we focus on the even fermionic parity sector spanned by $|00_g\rangle$ and $|11_g\rangle$, the unitary transformation becomes

$$U = \frac{1}{\sqrt{2}} \begin{pmatrix} 1 & -1 \\ 1 & 1 \end{pmatrix}. \quad (8)$$

Therefore, the braiding of A and C corresponds to a Hadamard gate operation on the basis of $|00_g\rangle$ and $|11_g\rangle$. Similar analysis is applicable to the $(-\frac{\pi}{4})$ -phase gate and the $\frac{\pi}{8}$ -phase gate, as shown in the Supplementary Information.

AUTHOR CONTRIBUTIONS

Y.-J.H. constructed the theoretical scheme. J.-S.X. and K.S. designed the experiment. K.S. performed the experiment with the assistant of J.-S.X.. J.K.P. contributed to the theoretical analysis. J.-S.X., K.S., Y.-J.H. and J.K.P. wrote the manuscript. Y.-J.H. supervised the theoretical part of the project. C.-F.L. and G.-C.G. supervised the project. All authors read the paper and discussed the results.

ACKNOWLEDGMENTS

This work was supported by the National Key Research and Development Program of China (Grants Number 2016YFA0302700), National Natural Science Foundation of China (Grant Numbers 61327901, 11325419, 11474267, 61322506, and 11274297), the Strategic Priority Research Program (B) of the Chinese Academy of Sciences (Grant Number XDB01030300), Key Research Program of Frontier Science, CAS (Grant Number QYZDY-SSW-SLH003), the Fundamental Research Funds for the Central Universities (Grant Number WK2470000020), Youth Innovation Promotion Association and Excellent Young Scientist Program CAS and the UK EPSRC grant EP/I038683/1.

ADDITIONAL INFORMATION

The authors declare no competing financial interests.

-
- [1] Shor, P. W. in *Proceedings of the 35th Annual Symposium on Foundations of Computer Science* (ed. Goldwasser, S.) 124-134 (IEEE Computer Society Press, 1994).
 - [2] Wilczek, F. & Zee, A. Appearance of gauge structure in simple dynamical systems. *Phys. Rev. Lett.* **52**, 2111-2114 (1984).

- [3] Nayak, C. Simon, S. H. Stern, A. Freedman, M. & Das Sarma, S. Non-abelian anyons and topological quantum computation. *Rev. Mod. Phys.* **80**, 1083-1159 (2008).
- [4] Das Sarma S., Freedman M., & Nayak C. Majorana zero modes and topological quantum computation. *NPJ quantum information* **1**, 15001 (2015).
- [5] Brown B. J., Loss D., Pachos J. K., Self C. & Wootton J. R. Quantum memories at finite temperature. *Rev. Mod. Phys.* **88**, 045005 (2016).
- [6] J. K. Pachos, *Introduction to Topological Quantum Computation*, Cambridge University Press (2012).
- [7] Das Sarma S, Freedman M, Nayak C. Topologically protected qubits from a possible non-Abelian fractional quantum Hall state. *Phys. Rev. Lett.* **94**, 166802 (2005).
- [8] Sau, J. D. Lutchyn, R. M. Tewari, S. & Das Sarma, S. Generic new platform for topological quantum computation using semiconductor heterostructures, *Phys. Rev. Lett.* **104**, 040502 (2010).
- [9] Lutchyn R. M., Sau J. D., Das Sarma S. Majorana fermions and a topological phase transition in semiconductor-superconductor heterostructures. *Phys. Rev. Lett.* **105**, 077001 (2010).
- [10] Fu, L. & Kane, C. Superconducting proximity effect and Majorana fermions at the surface of a topological insulator. *Phys. Rev. Lett.* **100**, 096407 (2008).
- [11] Mourik, V. *et al.* Signatures of Majorana fermions in hybrid superconductor-semiconductor nanowire devices. *Science* **336**, 1003-1007 (2012).
- [12] Deng, M. T. *et al.* Anomalous zero-bias conductance peak in a Nb-InSb nanowire-Nb hybrid device. *Nano. Lett.* **12**, 6414-6419 (2012).
- [13] Rokhinson, L. P. Liu, X. & Furdyna, J. K. The fractional a.c. Josephson effect in a semiconductor-superconductor nanowire as a signature of Majorana particles. *Nature Phys.* **8**, 795-799 (2012).
- [14] Mebrahtu, H. T. *et al.* Observation of Majorana quantum critical behaviour in a resonant level coupled to a dissipative environment. *Nature Phys.* **9**, 732-737 (2013).
- [15] Nadj-Perge, S. *et al.* Observation of Majorana fermions in ferromagnetic atomic chains on a superconductor. *Science* **346**, 602-607 (2014).
- [16] Lee, E. J. H. *et al.* Spin-resolved Andreev levels and parity crossings in hybrid superconductor-semiconductor nanostructures. *Nature Nano.* **9**, 79-84 (2014).

- [17] Xu, J.-P. *et al.* Experimental detection of a Majorana mode in the core of a Magnetic vortex inside a topological insulator-superconductor $\text{Bi}_2\text{Te}_3/\text{NbSe}_2$ Heterostructure. *Phys. Rev. Lett.* **114**, 017001 (2015).
- [18] Sun, H.-H. *et al.* Majorana zero mode detected with spin selective Andreev reflection in the vortex of a topological superconductor. *Phys. Rev. Lett.* **116**, 257003 (2016).
- [19] Aspuru-guzik, A. & Walther P. Photonic quantum simulators. *Nature Phys.* **8**, 285-291 (2012).
- [20] Jordan, P. & Wigner, E. Uber das Paulische Equivalenzverbot. *Z. Phys.* **47**, 631-651 (1928).
- [21] Kitaev, A. & Laumann, C. ‘Topological phases and quantum computation’ in Les Houches Summer School ‘Exact methods in low-dimensional physics and quantum computing’ (2008).
- [22] Bravyi S. Universal quantum computation with the $\nu = 5/2$ fractional quantum Hall state. *Phys. Rev. A* **73**, 042313 (2006).
- [23] Gottesman, D. *Proceedings of the XXII International Colloquium on Group Theoretical Methods in Physics*, eds. S. P. Corney, R. Delbourgo, and P. D. Jarvis, pp. 32-43 (Cambridge, MA, International Press, 1999).
- [24] Bonderson P., Clarke D. J., Nayak C., & Shtengel K., Implementing arbitrary gates with Ising anyons. *Phys. Rev. Lett.* **104**, 180505 (2010)
- [25] Bravyi S, Kitaev A. Universal quantum computation with ideal Clifford gates and noisy ancillas. *Phys. Rev. A* **71**, 022316 (2005).
- [26] Kliuchnikov V, Maslov D, Mosca M. Fast and efficient exact synthesis of single qubit unitaries generated by Clifford and T gates. *Quantum Inf. Comput.* **13**, 607-630 (2013).
- [27] Paetznick A, Svore K. Repeat-until-success: Non-deterministic decomposition of single-qubit unitaries. *Quantum Inf. Comput.*, **14**, 1277-1301 (2014).
- [28] Deutsch, D. & Jozsa, R. Rapid solution of problems by quantum computation. *Proc. R. Soc. Lond. A* **439**, 553-558 (1992).
- [29] Kraus, C. V. Zoller P. & Baranov, M. A. Braiding of Atomic Majorana Fermions in Wire Networks and Implementation of the Deutsch-Jozsa Algorithm. *Phys. Rev. Lett.* **111**, 203001 (2013).
- [30] Kitaev, A. Y. Unpaired Majorana fermions in quantum wires. *Phys.-Usp.* **44**, 131-136 (2001).
- [31] Xu, J.-S., Sun, K., Han, Y.-J., Li, C.-F., J. K. Pachos, and Guo, G.-C. Simulating the exchange of Majorana zero modes with a photonic system. *Nat. Commun.* **7**, 13194 (2016).

- [32] Kitagawa, T. *et al.* Observation of topologically protected bound states in photonic quantum walks. *Nat. Commun.* **3**, 882 (2012).
- [33] O'Brien, J. L., Pryde, G. J., Gilchrist, A., James, D. F. V., Langford, N. K., Ralph, T. C. & White, A. G., Quantum process tomography of a controlled-NOT gate. *Phys. Rev. Lett.* **93**, 080502 (2004).
- [34] Barreiro, J. T. *et al.* An open-system quantum simulator with trapped ions. *Nature* **470**, 486C491 (2011).
- [35] Daley A. J., Quantum trajectories and open many-body quantum systems. *Adv. Phys.* **63**, 77-149 (2014).

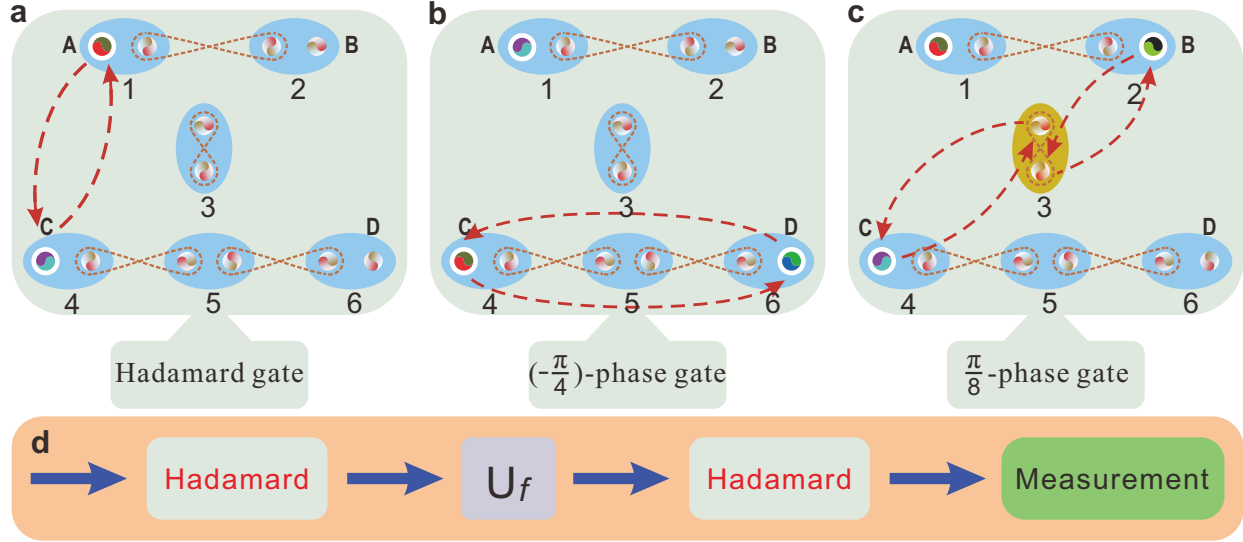


FIG. 1. The set of universal quantum gates and the Deutsch-Jozsa algorithm. The Kitaev chains consist of six fermions (numbered from 1 to 6) with four endpoint Majorana zero modes A, B, C and D, which can be used to demonstrate the universal gates. Each two Majorana fermions in the blue ellipse form a conventional fermion. The dashed lines between different Majorana fermions represent the initial interactions between them. **a.** The anticlockwise braiding of Majoranas A and C, implements a Hadamard gate, H , acting on the logical qubit. **b.** The anticlockwise braiding of Majoranas C and D, implements a $(-\frac{\pi}{4})$ -phase gate, R , acting on the logical qubit. **c.** The real time population-dependent evolution on Majoranas B and C, which is realised by transporting the two MZMs to a single site (site 3 in our experiment) and applying a coupling between them, leads to a $\frac{\pi}{8}$ -phase gate, T , acting on the logical qubit. **d.** The process that implements the Deutsch-Jozsa algorithm in a topologically protected manner. The Hadamard gate is implemented by anticlockwise braiding A and C. The unitary operation, U_f , considered as a black box whose character needs to be determined, can be either the identity (corresponding to the constant function) or the σ_z operation which can be implemented by two successive braiding of C and D (corresponding to the balanced function).

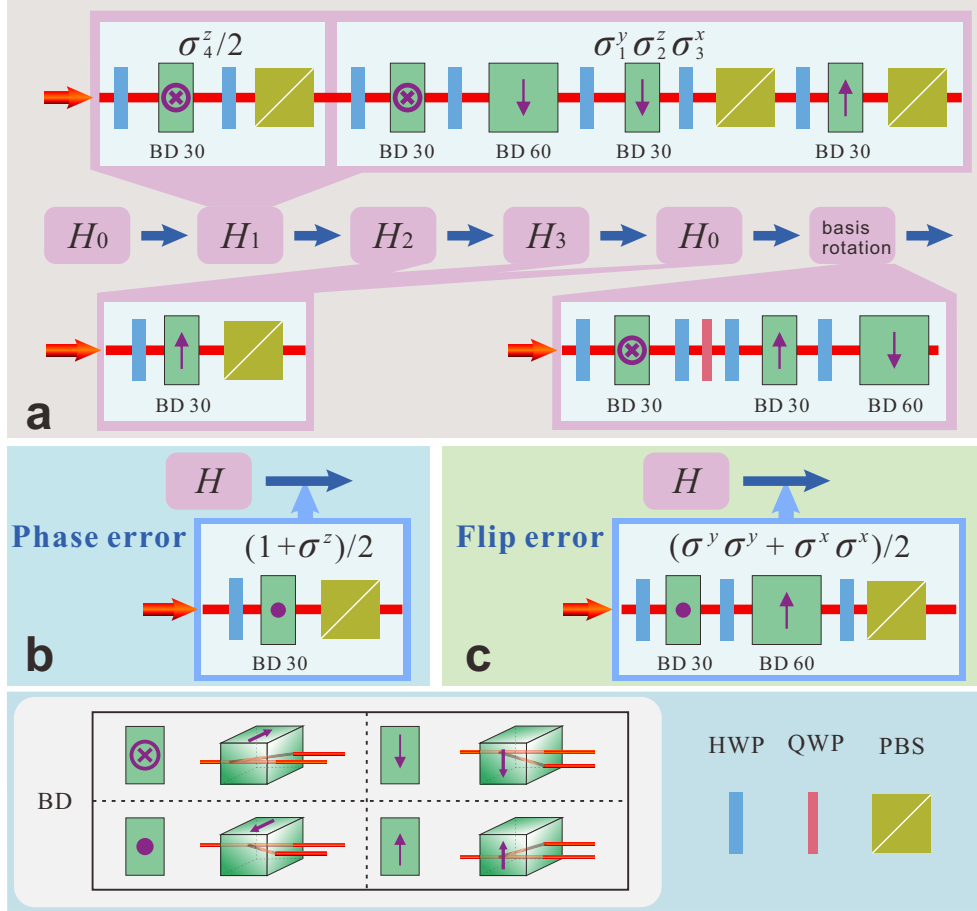


FIG. 2. Experimental setup. **a**. Experimental setup for the exchange of A and C. The imaginary-time evolutions of the involved Hamiltonians are realised in the panels. Half-wave plates (HWP), quarter-wave plates (QWP) and beam displacers (BDs) are used to rotate the states in the basis of the eigenstates of the corresponding Hamiltonian. The dissipative evolution is carried out by polarisation beam splitters (PBSs). By appropriately setting the axis of BDs, photons separate in different directions. **b**. and **c**. The setups that simulate the phase error and flip error.

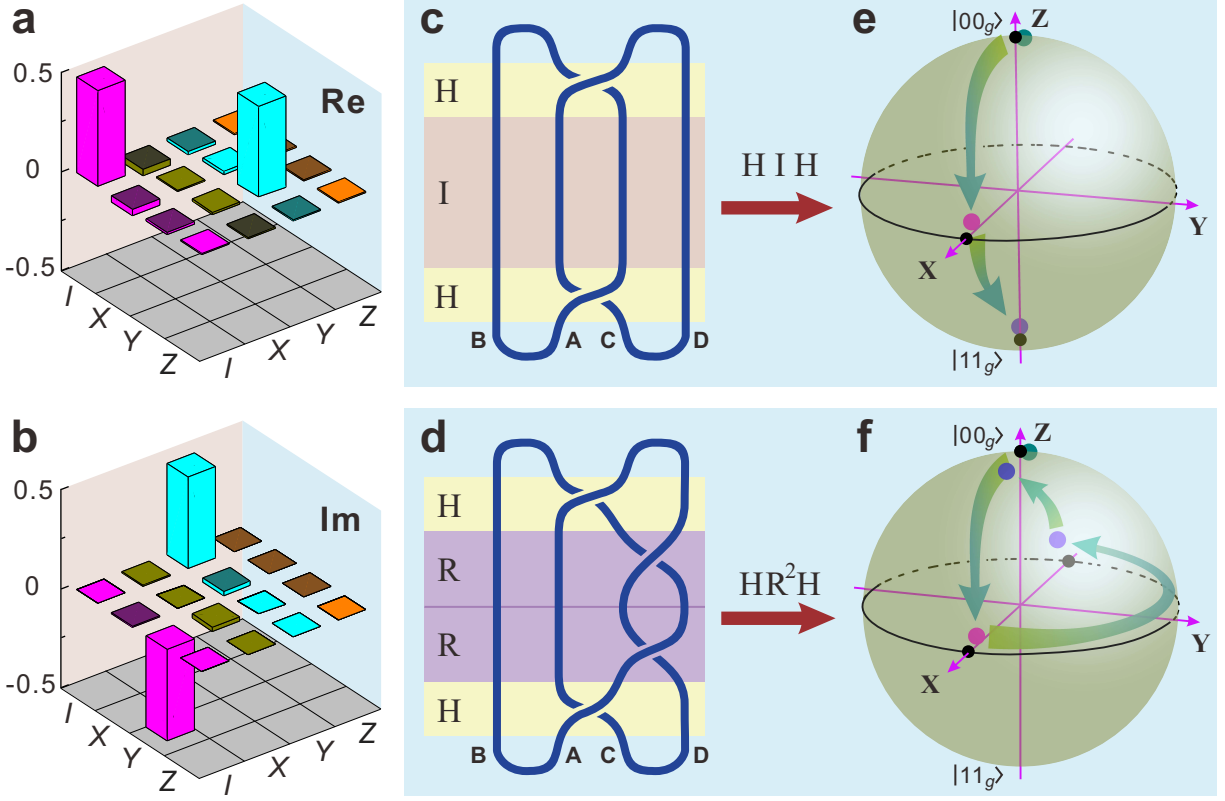


FIG. 3. Experimentally obtained density matrices from the Hadamard gate operation and the state evolution in the Deutsch-Jozsa algorithm. **a.** Real (Re) and **b.** Imaginary (Im) parts of the Hadamard gate operator. The measurement basis of I, X, Y and Z represent the identity, σ^x , σ^y and σ^z , respectively, acting on the logical qubit. The possible evolutions of the initial state of $|00_g\rangle$ during the Deutsch-Jozsa algorithm are shown in **e** (Identity operation) and **f** (σ^z operation). Black dots are the theoretical predictions and coloured dots are the corresponding experimental results. The braiding patterns of the four MZMs A, B, C and D that correspond to the implementation of the Deutsch-Jozsa algorithm with U_f being the identity or the σ^z operation are shown in **c.** and **d.**, respectively.

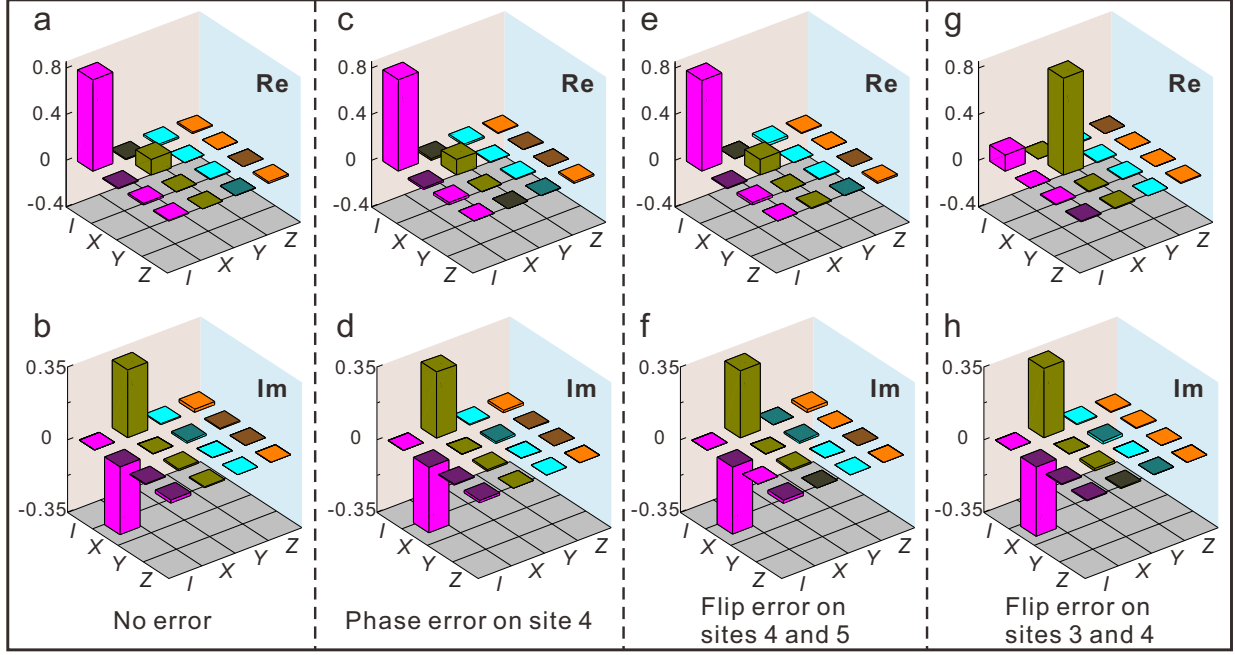


FIG. 4. Experimental results of the effect phase and flip errors have during the $\frac{\pi}{8}$ -phase gate on the logical qubit encoded in the basis $|00_g\rangle$ and $|11_g\rangle$. **a.** Real (Re) and **b.** Imaginary (Im) parts of the density matrix without errors. **c.** Real (Re) and **d.** Imaginary (Im) parts of the density matrix with phase error on site 4. **e.** Real (Re) and **f.** Imaginary (Im) parts of the density matrix with flip error on sites 4 and 5. **g.** Real (Re) and **h.** Imaginary (Im) parts of the density matrix with flip error on sites 3 and 4.